Abdominal Radiology (2019) 44:3295–3303
https://doi.org/10.1007/s00261-019-02079-z

SPLEEN

Measurement of spleen fat on MRI-proton density fat fraction arises from reconstruction of noise

Cheng William Hong[1,5] · Gavin Hamilton[1] · Catherine Hooker[1] · Charlie C. Park[1] · Calvin Andrew Tran[1] · Walter C. Henderson[1] · Jonathan C. Hooker[1] · Soudabeh Fazeli Dehkordy[1] · Jeffrey B. Schwimmer[2,3] · Scott B. Reeder[4] · Claude B. Sirlin[1,6]

Published online: 6 June 2019

Abstract

Purpose This study compares splenic proton density fat fraction (PDFF) measured using confounder-corrected chemical shift-encoded (CSE)-MRI to magnetic resonance spectroscopy (MRS) in human patients at 3T.

Methods This was a prospectively designed ancillary study to various previously described single-center studies performed in adults and children with known or suspected nonalcoholic fatty liver disease. Patients underwent magnitude-based MRI (MRI-M), complex-based MRI (MRI-C), high signal-to-noise variants (Hi-SNR MRI-M and Hi-SNR MRI-C), and MRS at 3T for spleen PDFF estimation. PDFF from CSE-MRI methods were compared to MRS-PDFF using Wilcoxon signed-rank tests. Demographics were summarized descriptively. Spearman's rank correlations were computed pairwise between CSE-MRI methods. Individual patient measurements were plotted for qualitative assessment. A significance level of 0.05 was used.

Results Forty-seven patients (20 female, 27 male) including 12 adults (median 55 years old) and 35 children (median 12 years old). Median PDFF estimated by MRS, MRI-M, Hi-SNR MRI-M, MRI-C, and Hi-SNR MRI-C was 1.0, 2.3, 1.9, 2.2, and 2.0%. The four CSE-MRI methods estimated statistically significant higher spleen PDFF values compared to MRS ($p < 0.0001$ for all). Pairwise associations in spleen PDFF values measured by different CSE-MRI methods were weak, with the highest Spearman's rank correlations being 0.295 between MRI-M and Hi-SNR MRI-M; none were significant after correction for multiple comparisons. No qualitative relationship was observed between PDFF measurements among the various methods.

Conclusion Overestimation of PDFF by CSE-MRI compared to MRS and poor agreement between related CSE-MRI methods suggest that non-zero PDFF values in human spleen are artifactual.

Keywords Spleen · Fat quantification · Spectroscopy · CSE-MRI · Artifactual

✉ Cheng William Hong
cwhong@ucsd.edu

✉ Claude B. Sirlin
csirlin@ucsd.edu

1 Liver Imaging Group, Department of Radiology, University of California San Diego, San Diego, CA, USA

2 Department of Pediatrics, School of Medicine, University of California San Diego, La Jolla, CA, USA

3 Department of Gastroenterology, Rady Children's Hospital San Diego, San Diego, CA, USA

4 Departments of Radiology, Medical Physics, Biomedical Engineering, Medicine, and Emergency Medicine, University of Wisconsin Madison, Madison, WI, USA

5 200 W. Arbor Drive #8756, San Diego, CA 92103-8756, USA

6 9500 Gilman Drive #0888, La Jolla, CA 92093-0888, USA

Introduction

Chemical shift-encoded (CSE)-MRI is an accurate method for the non-invasive in vivo measurement of proton density fat fraction (PDFF) in the liver [1–3]. This method is commonly used in the liver to assess hepatic steatosis and has high correlation with magnetic resonance spectroscopy (MRS), the reference standard for PDFF estimation [4–6].

The spleen generally has no detectable fat histologically except in very rare situations [7]. For this reason, it is sometimes used as a reference standard for calibration [1] and qualitatively as a comparison organ during subjective assessment of liver fat by radiologists [8]. In one report of six patients with iron overload with spleen PDFF measurements, the mean PDFF measured in the spleen was 2.1% [9]. Anecdotally, we have observed spleen CSE-MRI-PDFF

values greater than 4%, which is unexpected. The nature of these unexpectedly high PDFF measurements in the spleen is not well understood but may be artifactual. If so, it is possible that PDFF measurements of similar magnitude in other human tissues such as liver also may be artifactual.

In addition, PDFF and R2* have been previously shown to be correlated in the liver [10], however it is not known if PDFF and R2* values in the spleen exhibit a similar correlation.

Therefore, the purpose of this study is to assess whether splenic fat in human patients measured using CSE-MRI-PDFF is artifactual in patients using MRS as a reference standard, and to also assess the relationship between PDFF and R2* in the spleen.

Materials and methods

Study population

This was a prospectively designed ancillary study to various previously described single-center studies performed in adults and children with known or suspected nonalcoholic fatty liver disease (NAFLD) (references blinded during submission). The parent studies included two randomized clinical trials assessing pharmacologic intervention in hepatic steatosis [11, 12], a study designed to screen for NAFLD in high-risk patients [13], a study which assessed gut microbiome signatures to predict hepatic fibrosis [14], and a study of MR elastography in pediatric NAFLD. Those studies included four different CSE-MRI methods: magnitude-based (MRI-M), complex-based (MRI-C) methods, and high signal-to-noise (Hi-SNR) variants of both methods (Hi-SNR MRI M and Hi-SNR MRI-C) [15].

Consecutive participants in those studies who underwent CSE-MRI and MRS at 3T between April 2014 and July 2014 were enrolled for this ancillary study, which involved the addition of a breathhold MRS acquisition of the spleen. Children younger than 18 years signed informed assent with written informed consent provided by their parent(s)/guardian(s); adults signed informed consent. This study was approved by our Institutional Review Board, and compliant with the Health Insurance Portability and Accountability Act.

CSE-MRI examinations

Patients were imaged using a 3T MRI system (Signa EXCITE HDxt, GE Healthcare, Waukesha, WI) in the supine position with an eight-channel torso phased-array coil centered over the liver. A dielectric pad was placed between the coil and the abdomen. Each examination included single voxel MRS, and the following CSE-MRI acquisitions: MRI-M, Hi-SNR MRI-M, MRI-C, and Hi-SNR MRI-C. MRI methods assumed monoexponential R2* signal decay and applied a six-peak fat spectral model derived from human triglyceride composition [16]. A rectangular field of view was adjusted depending on body habitus and breath-hold capacity. The Hi-SNR methods obtained larger voxels by decreasing the matrix size, avoiding parallel imaging, and for MRI-C, by also decreasing the receiver bandwidth. Depending on the specific imaging parameters for any given patient, this resulted in an estimated SNR increase 2.0–2.4-fold for MRI-M and 3.1–3.5-fold for MRI-C. Previous studies have suggested that Hi-SNR methods may estimate PDFF with higher precision than standard methods, especially in the low PDFF range relevant to splenic measurements [15]. Acquisition parameters are summarized in Tables 1 and 2.

MRI-M and Hi-SNR MRI-M

A two-dimensional multi-echo spoiled gradient-recalled echo (SGRE) sequence was acquired with full liver and spleen coverage in one or two 20-s breath-holds. A low flip angle (10°) with ≥ 150 ms repetition time (TR) was used to minimize T1 bias [4, 5, 17, 18]. Six echoes were obtained per TR at nominally out-of-phase and in-phase echo times (based on a methylene resonance of 434 Hz relative to the water peak) of 1.15, 2.3, 3.45, 4.6, 5.75 and 6.9 ms to permit estimation of R2*-corrected PDFF and fat-corrected R2*. The rectangular field of view was adjusted depending on the patient's body habitus and breath-hold capacity. Externally calibrated parallel imaging (ASSET) with acceleration factor of 1.25 in the AP-direction was used for MRI-M. To increase SNR for the Hi-SNR MRI-M method, the voxel size was increased, the matrix size was decreased, and parallel imaging was not used [15]. A fitting algorithm was applied to the source images pixel by pixel to generate parametric PDFF and R2* maps [18]. Due to fat–water signal dominance ambiguity intrinsic to magnitude-based methods, water was assumed to be the dominant signal, and the PDFF dynamic range was limited to 0–50%. No corrections were necessary for phase errors [19, 20] as reconstruction of PDFF maps was performed with magnitude fitting.

MRI-C and Hi-SNR MRI-C

A three-dimensional multi-echo SGRE sequence was acquired with full liver and spleen coverage in a single 20-s breath hold. To minimize T1 bias, a low flip angle of 3° was used with a TR of 6–8 ms (Table 1) [21, 22]. Six echoes were obtained per TR at minimum TEs to optimize fat–water separation using complex-based methods [23]. Autocalibrated parallel imaging (ARC) was applied with an acceleration factor of 3.18. To increase SNR for the Hi-SNR MRI-C method, the voxel size was increased, the matrix

Table 1 MRI acquisition parameters

Parameter	MRI-M	Hi-SNR MRI-M	MRI-C	Hi-SNR MRI-C
Acquisition type	2D	2D	3D	3D
TR (ms)	150–250	225	5.7–7.2	6.1–6.2
TE (ms)	1.15, 2.3, 3.45, 4.6, 5.75, 6.9	1.15, 2.3, 3.45, 4.6, 5.75, 6.9	0.94, 1.7, 2.46, 3.21, 3.97, 4.72	0.78, 1.4, 2.02, 2.64, 3.26, 3.88
Matrix size	224 × 128–224 × 160	128 × 92	192 × 160	128 × 128
Bandwidth (kHz)	±142	±142	±125	±100
Flip angle (°)	10	10	3	3
Percent phase field of view (%)	65–100	65–80	65–90	70–90
Reconstruction diameter (mm)	380–440	380–440	380–440	400–440
Slice thickness (mm)	8–10	10	8	10
Number of averages	1	1	1	1
Parallel Imaging acceleration factor	1.25	Not used	3.18	Not used
Echo train length	6	6	3	3

MRI-M magnitude-based MRI, *MRI-C* complex-based MRI, *Hi-SNR* high signal-to-noise, *TR* relaxation time, *TE* echo time

Table 2 MRS acquisition parameters

Parameter	MRS
TR (ms)	150–2000
TE (ms)	10–110
TM (ms)	5
Flip angle (°)	90
Voxel size	15 × 15 × 15 mm^3

TR relaxation time, *TE* echo time, *TM* mixing time

size was decreased, the receiver bandwidth was reduced, and parallel imaging was not used. The iterative decomposition of water and fat with echo asymmetry and least-squares estimation method was used to generate PDFF and R2* maps [23–26]. This hybrid approach corrects for phase errors that may affect pure complex fitting [27]. The incorporation of phase data allows unambiguous fat–water separation and provides a full PDFF dynamic range of 0–100%.

MR spectroscopy

Multi-TR, multi-TE MRS was performed with a 15 × 15 × 15 mm^3 voxel in the spleen using the stimulated echo acquisition mode sequence (Fig. 1) [28]. This sequence acquires 32 spectra in a 21 s breath-hold with a range of TR and TE values allowing accurate estimation of T1 and T2 of both water and fat as well as accurate estimation of T1- and T2-corrected PDFF [28]. Spectra collected from each of the eight surface coil elements were combined using singular value decomposition [29]. An MR physicist (initials blinded during submission, > 15 years of experience) blinded to the MRI acquisitions performed the analysis using the Advanced Method for Accurate, Robust, and Efficient Spectral fitting of MRS data (AMARES) [30] included in Java-based magnetic resonance user interface software package [31]. The fat peaks were fitted by a single Gaussians assuming a previously established fat spectrum [16]. The frequency and amplitude of the fat peaks were fixed relative to each other, and assumed to have identical linewidth. Water was fitted by a single unconstrained Gaussian. A custom MATLAB routine nonlinearly fitted measured peak areas and reassigned fat included in the water peak using a previously established reference fat spectrum measured to estimate a T1-independent, and T2-corrected pre-contrast MRS-PDFF value [16]. Patients were excluded from this ancillary study if the voxel location overlapped surrounding adipose tissue or the voxel location could not be verified [28].

Image analysis

Image analysis was performed using OsiriX imaging software (Pixmeo, Geneva, Switzerland). In each patient, a single 1-cm-radius region-of-interest (ROI) was placed in the spleen co-localized to the MRS voxel avoiding major vessels, the spleen edge, and imaging artifacts. The fifth echo source image was used for ROI placement as it consistently provided adequate anatomical visualization [32]. The ROIs were then propagated to the PDFF maps to obtain PDFF values from each MRI method (Fig. 2). The ROIs were also propagated to the R2* maps to obtain R2* values in a similar manner. ROIs were placed on source (which provide no quantitative information on fat signal) rather than PDFF images to avoid feedback bias.

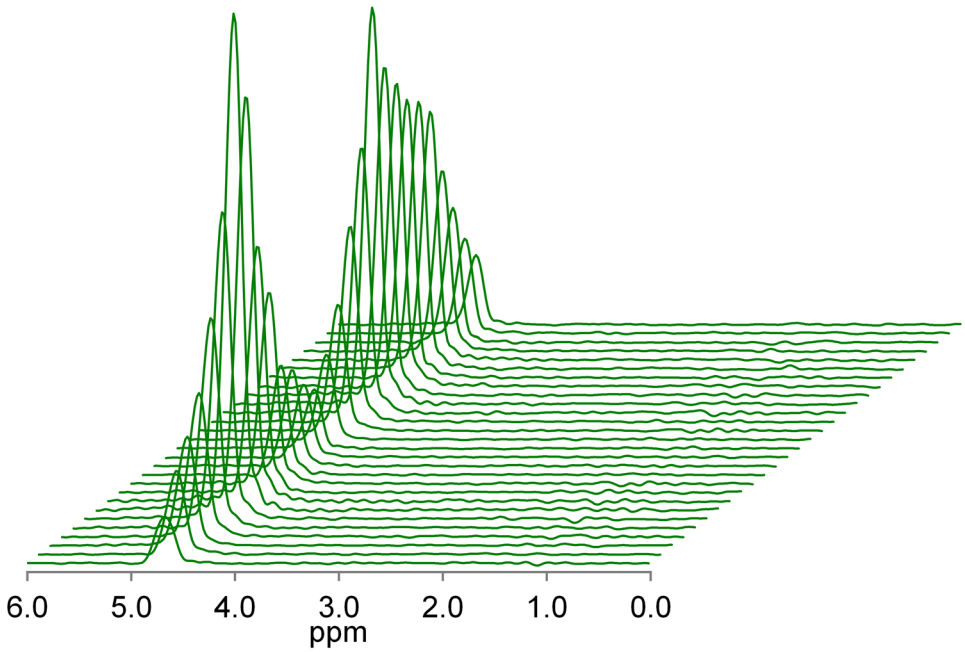

Fig. 1 Representative multi-TR, multi-TE MR spectrum of the spleen

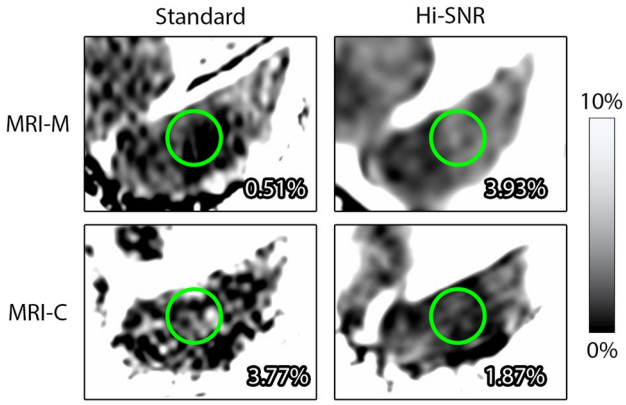

Fig. 2 Images from a 17-year-old female demonstrate how region-of-interest (ROI) placement on PDFF maps (green circles) allows for the measurement of PDFF from four CSE-MRI methods. As explained in the text, ROIs were placed on source images to avoid feedback bias and then propagated to the PDFF maps. The scale for all methods was windowed to 0–10% to illustrate low PDFF values in the spleen more clearly. All four CSE-MRE methods show low but positive spleen PDFF values, and the distribution of these positive spleen PDFF values is visibly different across these methods. PDFF measured by MRS was 0.37% in this patient. Notice the visibly higher SNR of the Hi-SNR images

Statistical analysis

Statistical analysis was performed using R version 3.3.3 statistical software (R: a language and environment for statistical computing. 2016. R Foundation for Statistical Computing, Vienna, Austria). Demographics were recorded and summarized descriptively. Spleen PDFF and R2* values were computed for each exam by taking the mean PDFF and R2* values of the pixels in the ROI.

As PDFF values obtained were right-skewed, the median, inter-quartile range (IQR), and range of PDFF values measured by each method was reported. PDFF values from the four CSE-MRI methods were compared to MRS-PDFF using Wilcoxon signed-rank tests. The pairwise Spearman's rank correlation coefficient was computed for each pair of CSE-MRI methods, and a scatterplot was generated of the pair of methods with the highest correlation for illustrative purposes. Spearman's rank correlation coefficient between PDFF and R2* was also computed for MRI-M and Hi-SNR MRI-M methods. The Holm–Bonferroni correction was applied to adjust for multiple comparisons. A significance level of 0.05 was used for all statistical testing.

In addition, a plot of individual patient measurements color-coded by rank order was generated for qualitative assessment.

Results

Cohort characteristics

Forty-eight patients underwent spleen MRI and MRS acquisitions during the study period. One patient was excluded as the location of the MRS voxel could not be verified to be within the spleen. The remaining 47 patients (20 female, 27 male) in this ancillary study included 12 adults (6 female, 6 male; median age 55 years, IQR 32–59 years) and 35

children (14 female, 21 male; median age 12 years, IQR 11–15 years). The range of ages was 8–65 years old.

Spleen PDFF

The median MRS-PDFF measured in the spleen was 1.0% (IQR 0.8–1.3%, range 0.5–3.6%). Using CSE-MRI, the median spleen PDFF measured using MRI-M, Hi-SNR MRI-M, MRI-C, and Hi-SNR MRI-C was 2.3% (IQR 1.9–2.8%, range 0.1–3.7%), 1.9% (IQR 1.6–2.6%, range − 0.1 to 4.1%), 2.2% (IQR 1.5–3.0%, range 0.4–5.8%), and 2.0% (IQR 1.6–2.5%, range 0.3–3.5%), respectively (Fig. 3). All four CSE-MRI methods estimated statistically significant higher spleen PDFF values compared to MRS (Wilcoxon signed rank tests, $p < 0.0001$ for all).

Correlation in spleen PDFF values measured by different CSE-MRI methods

Pairwise associations in spleen PDFF values measured by the different CSE-MRI methods were weak, with the highest Spearman's rank correlation coefficient being 0.295 between MRI-M and Hi-SNR MRI-M, and the lowest being − 0.039 between MRI-C and Hi-SNR MRI-C (Table 3). After

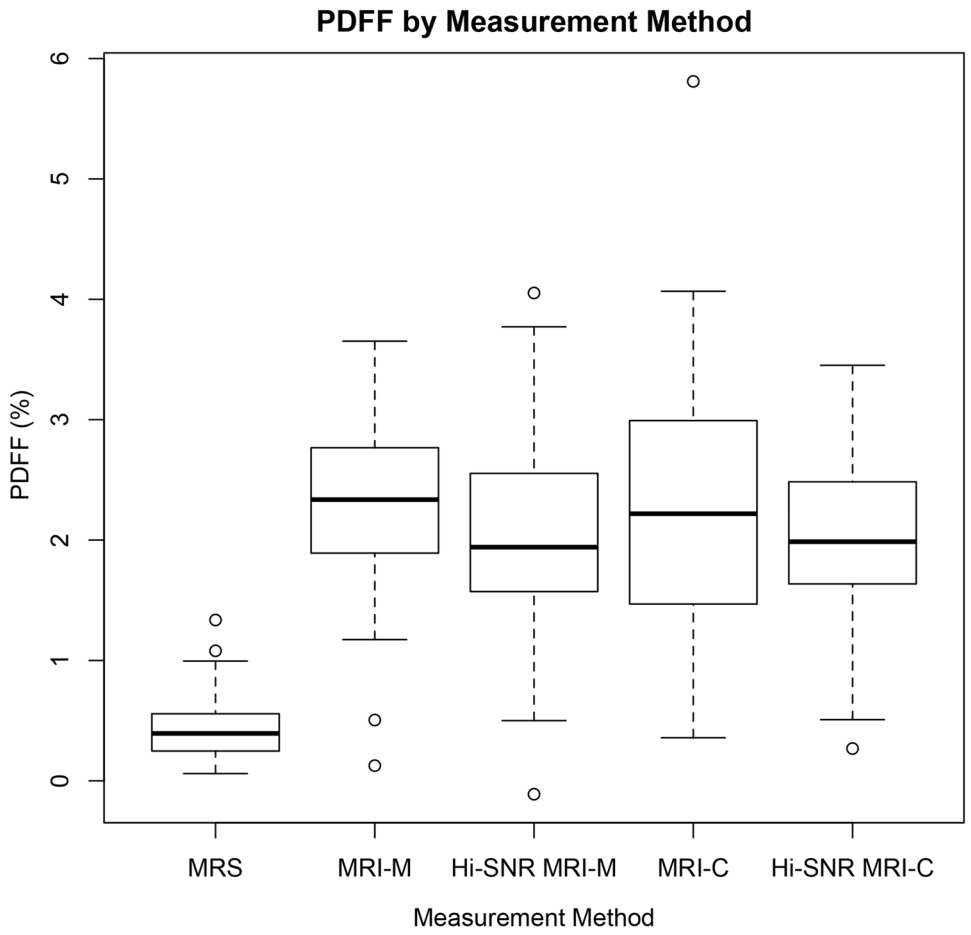

Fig. 3 PDFF values estimated all four CSE-MRI methods were significantly higher than PDFF estimated by MRS

Table 3 Matrix of pairwise Spearman's rank correlation coefficients among the four CSE-MRI-PDFF measurement methods

	MRI-M	Hi-SNR MRI-M	MRI-C	Hi-SNR MRI-C
MRI-M	–	0.295 ($p = 0.044$, 0.266)	0.262 ($p = 0.076$, 0.378)	0.066 ($p = 0.66$, 1.00)
Hi-SNR MRI-M		–	0.0943 ($p = 0.528$, 1.00)	0.166 ($p = 0.265$, 1.00)
MRI-C			–	− 0.039 ($p = 0.795$, 1.00)
Hi-SNR MRI-C				–

p values are included in parenthesis: the first number indicates the unadjusted *p* value, and the second indicates the adjusted *p* value after Holm–Bonferroni correction for multiple comparisons

MRI-M magnitude-based MRI, *MRI-C* complex-based MRI

Holm–Bonferroni correction for multiple comparisons, none of these associations were statistically significant.

As MRI-M and Hi-SNR MRI-M exhibited the highest rank correlation, a scatterplot of spleen PDFF measured by those two methods was generated for illustrative purposes, and no qualitative relationship was observed (Fig. 4). Similarly, a scatterplot of measurements by MRS and the four CSE-MRI methods shows that rank order of PDFF values is not preserved (Fig. 5).

Correlation between PDFF and R2*

All but one patient had MRI-M and Hi-SNR MRI-M splenic R2* estimates. Associations between splenic PDFF and R2* were relatively weak, with Spearman's rank correlations for MRI-M and Hi-SNR MRI-M being 0.42 and 0.05, respectively.

Discussion

This study demonstrates that CSE-MRI consistently provides positive PDFF values in the human spleen, despite the known rarity of fat deposition in this organ. All four CSE-MRI methods measured significantly higher PDFF compared to MRS. Additionally, the splenic PDFF values provided by four different CSE-MRI methods demonstrate poor agreement. The correlations between splenic PDFF and R2* values on MRI-M and Hi-SNR MRI-M were relatively weak and lower than the correlations reported in multiple prior studies where they ranging from 0.59 to 0.87 [10, 33, 34]. Taken together, these findings suggest that positive PDFF values measured in the spleen are artifactual rather than representing true fat signal.

There are several possibilities for these artifactual PDFF values. There may have been ghosting or aliasing of adipose tissue signal from other areas of the abdomen into the spleen, which may be imperceptible qualitatively. Alternatively or in combination, artifactual PDFF values may have arisen from noise, as noise floor effects are more pronounced at lower fat fractions [35]. This is especially true for

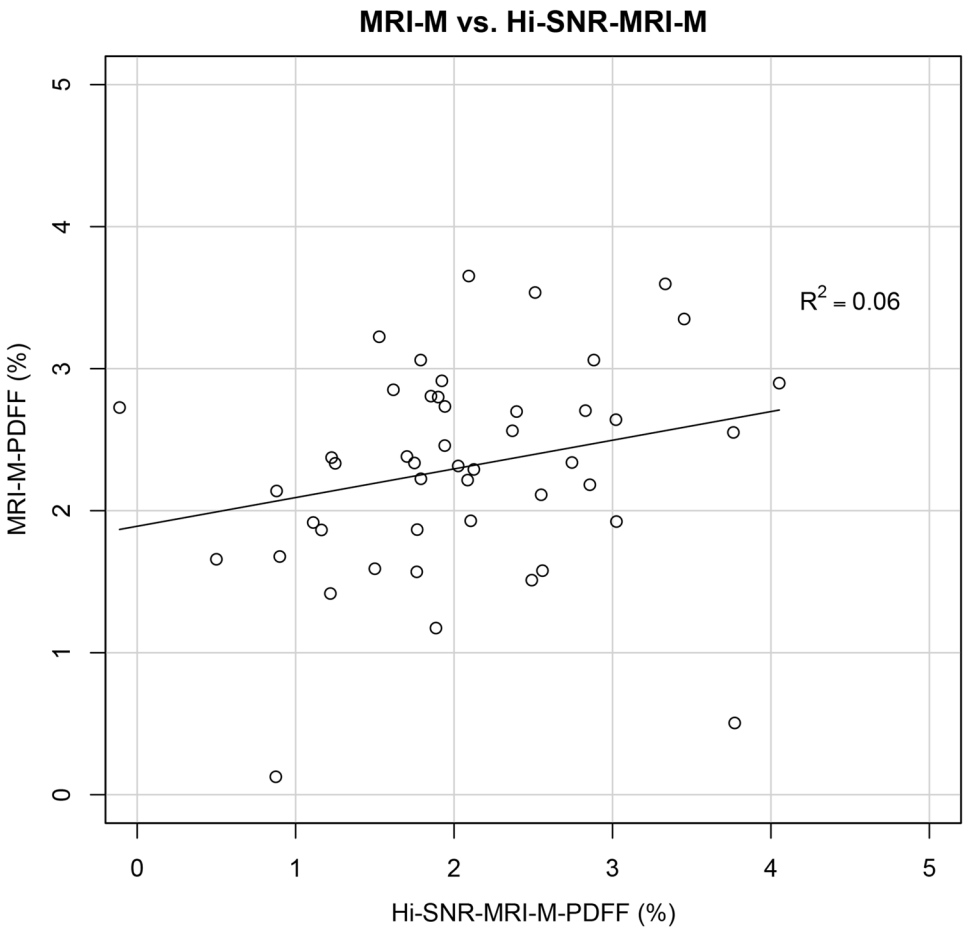

Fig. 4 Scatterplot demonstrates PDFF estimated by MRI-M versus Hi-SNR MRI-M. PDFF measurements were poorly correlated, and no relationship was clearly identified. The best-fit linear regression only achieved an $R^2 = 0.06$. Note that MRI-M and Hi-SNR MRI-M was the pair of methods with the highest rank correlation; other pairs had even weaker correlations and are not shown

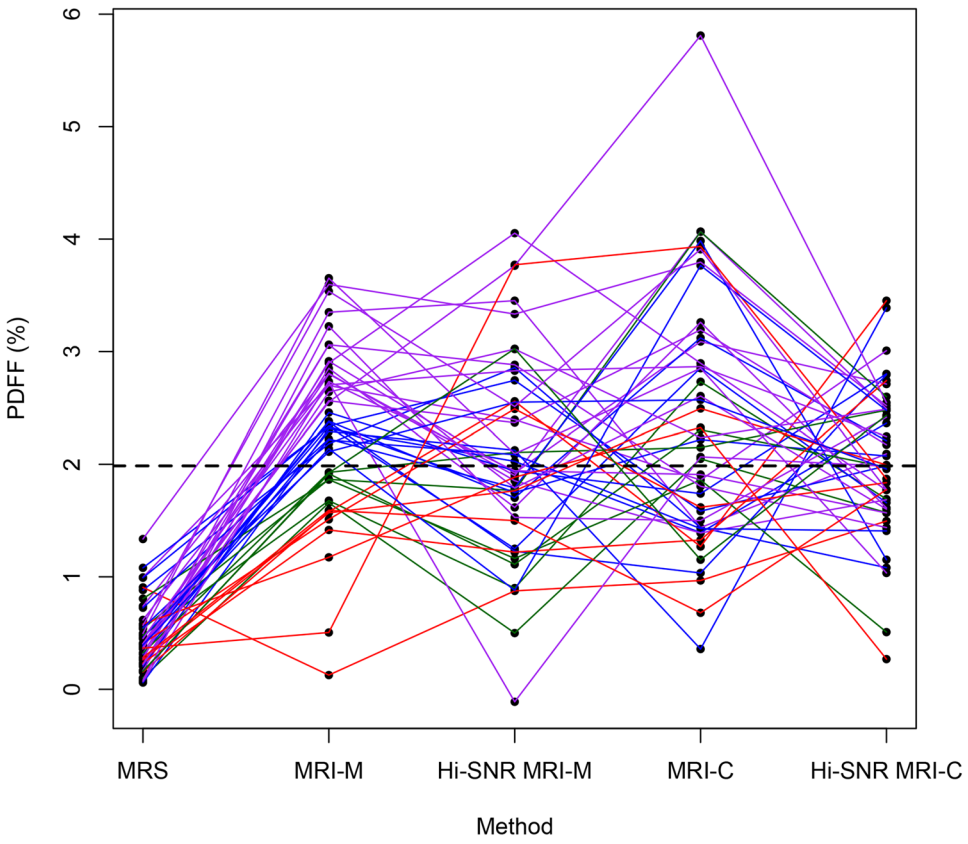

Fig. 5 Spleen PDFF measurements from each method. Each line represents an individual patient and the corresponding spleen PDFF values derived from each method. The black-dashed line indicates the median MRI-M PDFF, and the lines are color coded based on PDFF measured on MRI-M (first quartile: red, second quartile: green, third quartile: blue, fourth quartile: purple). Note that CSE-MRI consistently overestimates PDFF relative to MRS, and rank order is not preserved, with substantial relative differences in PDFF measured by different methods in the same patients

magnitude-based methods where areas of low fat signal have only positive noise after phase data is discarded, although modern methods have reduced this noise bias to less than 1% in the human liver [1, 36]. Unexpectedly, the artifactual PDFF values were not meaningfully reduced by using high-SNR methods, which may be because these variations in SNR are small compared to inherent noise. Another contributory factor for MRI-C methods could be concomitant gradients adding to phase error [37].

This study is the first to evaluate PDFF estimation compared to MRS in the spleen. In this cohort, the artifactual PDFF measured by various methods were about 2%, which raises the concern that there is a 2% bias in PDFF estimation by CSE-MRI in other organs, although this needs further validation. This is consistent with previous research showing that per-subject disagreement in hepatic PDFF estimation between MRI-M and MRI-C and between MRI-M and MRS ranges from about − 2 to 2%, which becomes more pronounced in the low PDFF range [20, 32, 38]. In combination with our results, these prior observations suggest that current CSE-MRI methods may have, on average, a 2% absolute error in PDFF estimation, which may challenge the interpretation of quantitative results in the low PDFF range. This is particularly relevant in the setting of a recent study by Nasr et al. suggesting that using a lower PDFF threshold of 3% for hepatic steatosis increases sensitivity without compromising specificity compared to a threshold of 5% [39]. Further research and technical innovations are needed to better understand the nature of noise and improve the accuracy of CSE-MRI-PDFF estimation in the low PDFF range. This range is relevant for epidemiology and genetics studies that use MRI-PDFF to classify research participants as having or not having NAFLD as well as for longitudinal research studies examining the resolution of hepatic steatosis. It is also relevant for emerging investigations of low-quantity fat deposition in other solid organs such as kidney [40, 41].

Limitations of this study include selection bias from analyzing research subjects at a single tertiary care facility and relatively small sample sizes, which may affect the generalizability of our results to populations in other geographical regions. Another limitation is the absence of histological confirmation, although splenic biopsy could not be justified in human subjects for this purpose.

In conclusion, the measurement of unexpected positive PDFF values in the spleen is in all likelihood, artifactual. Future research is needed to better understand the nature of these measurements and how they might impact clinical care and clinical research of low levels of fat deposition in liver, kidneys, and other solid organs.

Funding The authors would like to acknowledge Grant Support from the National Institutes of Health T32 EB005970-09, R01 DK106419-02, R01 DK083380, K24 DK102595, R01 DK088925, and R01 DK100651-03. We also acknowledge GE Healthcare who provides research support to UCSD and UW-Madison.

References

1. Reeder SB, Cruite I, Hamilton G, Sirlin CB. Quantitative assessment of liver fat with magnetic resonance imaging and spectroscopy. J Magn Reson Imaging. 2011;34(4):729–749.
2. Reeder SB, Hu HH, Sirlin CB. Proton density fat-fraction: a standardized MR-based biomarker of tissue fat concentration. J Magn Reson Imaging. 2012;36(5):1011–1014.
3. Meisamy S, Hines CDG, Hamilton G, et al. Quantification of hepatic steatosis with T1-independent, T2-corrected MR imaging with spectral modeling of fat: blinded comparison with MR spectroscopy. Radiology. 2011;258(3):767–775.
4. Yokoo T, Shiehmorteza M, Hamilton G, et al. Estimation of hepatic proton-density fat fraction by using MR imaging at 3.0 T. Radiology. 2011;258(3):749–759.
5. Yokoo T, Bydder M, Hamilton G, et al. Nonalcoholic fatty liver disease: diagnostic and fat-grading accuracy of low-flip-angle multiecho gradient-recalled-echo MR imaging at 1.5 T. Radiology. 2009;251(1):67–76.
6. Hernando D, Sharma SD, Aliyari Ghasabeh M, et al. Multisite, multivendor validation of the accuracy and reproducibility of proton-density fat-fraction quantification at 1.5T and 3T using a fat-water phantom. Magn Reson Med. 2016
7. Forbes GB. Splenic lipidosis after administration of intravenous fat emulsions. J Clin Pathol. 1978;31(8):765–771.
8. Cassidy FH, Yokoo T, Aganovic L, et al. Fatty Liver Disease: MR Imaging Techniques for the Detection and Quantification of Liver Steatosis. RadioGraphics. Radiological Society of North America; 2009;29(1):231–260.
9. İdilman İS, Gümrük F, Haliloğlu M, Karçaaltıncaba M. The Feasibility of Magnetic Resonance Imaging for Quantification of Liver, Pancreas, Spleen, Vertebral Bone Marrow, and Renal Cortex R2* and Proton Density Fat Fraction in Transfusion-Related Iron Overload. Turkish J Haematol Off J Turkish Soc Haematol. Galenos Yayinevi; 2016;33(1):21–27.
10. Mamidipalli A, Hamilton G, Manning P, et al. Cross-sectional correlation between hepatic R2* and proton density fat fraction (PDFF) in children with hepatic steatosis. J Magn Reson Imaging. 2018;47(2):418–424.
11. Loomba R, Sirlin CB, Ang B, et al. Ezetimibe for the treatment of nonalcoholic steatohepatitis: assessment by novel magnetic resonance imaging and magnetic resonance elastography in a randomized trial (MOZART trial). Hepatology. 2015;61(4):1239–1250.
12. Cui J, Philo L, Nguyen P, et al. Sitagliptin vs. placebo for non-alcoholic fatty liver disease: A randomized controlled trial. J Hepatol. 2016;65(2):369–376.
13. Doycheva I, Cui J, Nguyen P, et al. Non-invasive screening of diabetics in primary care for NAFLD and advanced fibrosis by MRI and MRE. Aliment Pharmacol Ther. NIH Public Access; 2016;43(1):83–95.
14. Loomba R, Seguritan V, Li W, et al. Gut Microbiome-Based Metagenomic Signature for Non-invasive Detection of Advanced Fibrosis in Human Nonalcoholic Fatty Liver Disease. Cell Metab. 2017;25(5):1054–1062.e5.
15. Motosugi U, Hernando D, Wiens C, Bannas P, Reeder SB. High SNR Acquisitions Improve the Repeatability of Liver Fat Quantification Using Confounder-corrected Chemical Shift-encoded MR Imaging. Magn Reson Med Sci. 2017
16. Hamilton G, Yokoo T, Bydder M, et al. In vivo characterization of the liver fat ^{1}H MR spectrum. NMR Biomed. 2011;24(7):784–790.
17. Kühn J-P, Hernando D, Mensel B, et al. Quantitative chemical shift-encoded MRI is an accurate method to quantify hepatic steatosis. J Magn Reson Imaging. 2014;39(6):1494–1501.
18. Bydder M, Yokoo T, Hamilton G, et al. Relaxation effects in the quantification of fat using gradient echo imaging. Magn Reson Imaging. 2008;26(3):347–359.
19. Hernando D, Hines CDG, Yu H, Reeder SB. Addressing phase errors in fat-water imaging using a mixed magnitude/complex fitting method. Magn Reson Med. NIH Public Access; 2012;67(3):638–644.
20. Yu H, Shimakawa A, Hines CDG, et al. Combination of complex-based and magnitude-based multiecho water-fat separation for accurate quantification of fat-fraction. Magn Reson Med. 2011;66(1):199–206.
21. Kühn J-P, Jahn C, Hernando D, et al. T1 bias in chemical shift-encoded liver fat-fraction: Role of the flip angle. J Magn Reson Imaging. 2014;40(4):875–883.
22. Johnson BL, Schroeder ME, Wolfson T, et al. Effect of flip angle on the accuracy and repeatability of hepatic proton density fat fraction estimation by complex data-based, T1-independent, T2*-corrected, spectrum-modeled MRI. J Magn Reson Imaging. 2014;39(2):440–447.
23. Reeder SB, Pineda AR, Wen Z, et al. Iterative decomposition of water and fat with echo asymmetry and least-squares estimation (IDEAL): application with fast spin-echo imaging. Magn Reson Med. 2005;54(3):636–644.
24. Reeder SB, McKenzie CA, Pineda AR, et al. Water–fat separation with IDEAL gradient-echo imaging. J Magn Reson Imaging. 2007;25(3):644–652.
25. Reeder SB, Wen Z, Yu H, et al. Multicoil Dixon chemical species separation with an iterative least-squares estimation method. Magn Reson Med. 2004;51(1):35–45.
26. Hernando D, Haldar JP, Sutton BP, Ma J, Kellman P, Liang Z-P. Joint estimation of water/fat images and field inhomogeneity map. Magn Reson Med. 2008;59(3):571–580.
27. Yu H, Shimakawa A, McKenzie CA, Brodsky E, Brittain JH, Reeder SB. Multiecho water-fat separation and simultaneous R2* estimation with multifrequency fat spectrum modeling. Magn Reson Med. NIH Public Access; 2008;60(5):1122–1134.
28. Hamilton G, Middleton MS, Hooker JC, et al. In vivo breath-hold (1) H MRS simultaneous estimation of liver proton density fat fraction, and T1 and T2 of water and fat, with a multi-TR, multi-TE sequence. J Magn Reson Imaging. 2015;42(6):1538–1543.
29. Bydder M, Hamilton G, Yokoo T, Sirlin CB. Optimal phased-array combination for spectroscopy. Magn Reson Imaging. 2008;26(6):847–850.
30. Vanhamme, van den Boogaart A, Van Huffel S. Improved method for accurate and efficient quantification of MRS data with use of prior knowledge. J Magn Reson. 1997;129(1):35–43.
31. Naressi A, Couturier C, Devos JM, et al. Java-based graphical user interface for the MRUI quantitation package. MAGMA. 2001;12(2–3):141–152.
32. Haufe WM, Wolfson T, Hooker CA, et al. Accuracy of PDFF estimation by magnitude-based and complex-based MRI in children with MR spectroscopy as a reference. J Magn Reson Imaging. 2017
33. Bashir MR, Huang R, Mayes N, et al. Concordance of hypervascular liver nodule characterization between the organ procurement and transplant network and liver imaging reporting and data system classifications. J Magn Reson Imaging. 2015;42(2):305–314.

34. Karlsson M, Ekstedt M, Dahlström N, et al. Liver R2* is affected by both iron and fat: A dual biopsy-validated study of chronic liver disease. J Magn Reson Imaging. 2019
35. Roberts NT, Hernando D, Holmes JH, Wiens CN, Reeder SB. Noise properties of proton density fat fraction estimated using chemical shift-encoded MRI. Magn Reson Med. 2018;80(2):685–695.
36. Liu C-Y, McKenzie CA, Yu H, Brittain JH, Reeder SB. Fat quantification with IDEAL gradient echo imaging: correction of bias from T(1) and noise. Magn Reson Med. 2007;58(2):354–364.
37. Colgan TJ, Hernando D, Sharma SD, Reeder SB. The effects of concomitant gradients on chemical shift encoded MRI. Magn Reson Med. 2017;78(2):730–738.
38. Yokoo T, Serai SD, Pirasteh A, et al. Linearity, Bias, and Precision of Hepatic Proton Density Fat Fraction Measurements by Using MR Imaging: A Meta-Analysis. Radiology. 2017;170550.
39. Nasr P, Forsgren MF, Ignatova S, et al. Using a 3% Proton Density Fat Fraction as a Cut-Off Value Increases Sensitivity of Detection of Hepatic Steatosis, Based on Results From Histopathology Analysis. Gastroenterology. 2017;153(1):53–55.e7.
40. Idilman IS, Tuzun A, Savas B, et al. Quantification of liver, pancreas, kidney, and vertebral body MRI-PDFF in non-alcoholic fatty liver disease. Abdom Imaging. 2015;40(6):1512–1519.
41. Hong CW, Fazeli Dehkordy S, Hooker JC, Hamilton G, Sirlin CB. Fat Quantification in the Abdomen. Top Magn Reson Imaging. 2017;26(6):221–227.